Is there a tropical response to recent observed Southern Ocean cooling?

Xiyue Zhang[1], Clara Deser[2], and Lantao Sun[3]

[1]National Center for Atmospheric Research
[2]National Center for Atmospheric Research (UCAR)
[3]Colorado State University

November 26, 2022

Abstract

Despite global warming, SSTs in the Southern Ocean (SO) have cooled in recent decades largely as a result of internal variability. The global impact of this cooling is assessed by nudging evolving SO SST anomalies to observations in an ensemble of coupled climate model simulations under historical radiative forcing, and comparing against a control ensemble. The most significant remote response to observed SO cooling is found in the tropical South Atlantic, where increased clouds and strengthened trade winds cool the sea surface, partially offsetting the radiatively-forced warming trend. The SO ensemble produces a more realistic tropical South Atlantic SST trend, and exhibits a higher pattern correlation with observed SST trends in the greater Atlantic basin, compared to the control ensemble. SO cooling also produces a significant increase in Antarctic sea ice, but not enough to offset radiatively-induced ice loss; thus, the SO ensemble remains biased in its sea ice trends.

Is there a tropical response to recent observed Southern Ocean cooling?

Xiyue Zhang[1], Clara Deser[1], and Lantao Sun[2]

[1]National Center for Atmospheric Research, Boulder, Colorado, USA
[2]Colorado State University, Fort Collins, Colorado, USA

Key Points:

- The global impact of recent observed Southern Ocean surface cooling is studied using coupled model experiments in a Pacemaker framework
- Southern Ocean cooling induces significant cooling of the tropical South Atlantic via increased cloudiness and strengthened trade winds
- It also slows down the rate of radiatively-induced Antarctic sea ice loss, although model disagreement with observed ice expansion remains

Corresponding author: Xiyue Zhang, `sallyz@ucar.edu`

Abstract

Despite global warming, SSTs in the Southern Ocean (SO) have cooled in recent decades largely as a result of internal variability. The global impact of this cooling is assessed by nudging evolving SO SST anomalies to observations in an ensemble of coupled climate model simulations under historical radiative forcing, and comparing against a control ensemble. The most significant remote response to observed SO cooling is found in the tropical South Atlantic, where increased clouds and strengthened trade winds cool the sea surface, partially offsetting the radiatively-forced warming trend. The SO ensemble produces a more realistic tropical South Atlantic SST trend, and exhibits a higher pattern correlation with observed SST trends in the greater Atlantic basin, compared to the control ensemble. SO cooling also produces a significant increase in Antarctic sea ice, but not enough to offset radiatively-induced ice loss; thus, the SO ensemble remains biased in its sea ice trends.

Plain Language Summary

Understanding how the observed pattern of global sea surface temperatures (SST) changes come about remains a key objective in climate science. SSTs are expected to rise as greenhouse gas concentrations increase. However, from 1979 to 2013, SSTs in the Southern Ocean cooled because of natural climate variability, accompanied by Antarctic sea ice expansion. Yet this cooling and sea ice expansion are not generally captured by climate models. In this study, we artificially incorporate the observed Southern Ocean cooling in a climate model to see how it affects SSTs in other regions. We found that in response to Southern Ocean cooling, the tropical South Atlantic SST cools and Antarctic sea ice expands, similar to observations. However, in simulations without the Southern Ocean cooling, the Atlantic SST response look distinctly different, and Antarctic sea ice retreats significantly. Our study suggests that realistic simulation of internal decadal SO SST variability may be important for credible decadal SST projections in the tropical South Atlantic.

1 Introduction

Observed global sea surface temperature (SST) trends in recent decades show a distinctive spatial pattern, with warming in the western Pacific, Indian Ocean, and North Atlantic, and cooling in the eastern Pacific, South Atlantic, and Southern Ocean (SO, Figure 1a). This pattern is reminiscent of both the Pacific Decadal Oscillation/Interdecadal Pacific Oscillation (PDO/IPO) (Mantua et al., 1997; Power et al., 1999) and the Atlantic Multidecadal Oscillation (AMO) (Kerr, 2000; Enfield et al., 2001), the dominant modes of internal low frequency variability over the Pacific and Atlantic sectors, respectively. The cooling over the SO has been partially attributed to internal variability associated with changes in deep water formation (Latif et al., 2013; Cabré et al., 2017; Kostov et al., 2018; L. Zhang et al., 2019), in addition to contributions from ozone depletion (Ferreira et al., 2014) and melting of the Antarctic ice sheet (Bintanja et al., 2013; Bronselaer et al., 2018).

While the role of the tropics in extra-tropical climate variability is well established (Alexander et al., 2002; Deser et al., 2004; Kosaka & Xie, 2013; Newman et al., 2016), the extra-tropics may also influence the tropics via coupled air-sea interactions. For example, midlatitude atmospheric variability can effectively provide stochastic forcing for ENSO via the "seasonal footprinting mechanism" (Vimont et al., 2003; Alexander et al., 2010) and via the "meridional mode" (H. Zhang et al., 2014; Amaya et al., 2019); the latter may also play a role in tropical Pacific decadal variability (Sun & Okumura, 2019; Liguori & Di Lorenzo, 2019).

At high latitudes, projected sea ice loss in both hemispheres has been shown to impact the tropical Pacific via dynamical and thermodynamic air-sea interaction processes, although the detailed mechanisms are not yet fully understood (Deser et al., 2015; K. Wang et al., 2018; England et al., 2020). SO SST variability resulting from open-ocean convection in Weddell Sea has a significant impact on global energy balance redistribution, affecting tropical SSTs and precipitation (Cabré et al., 2017). Idealized studies have explored the effects of SO SST cooling, which often extends into the tropical southeastern Pacific and Atlantic (Hwang et al., 2017; Kang et al., 2019), reducing the warm SST biases in those regions (Mechoso et al., 2016). Hwang et al. (2017) attributed the zonal asymmetry in the tropical South Pacific SST response to wind-evaporation-SST (WES) and shortwave cloud feedbacks, while ocean dynamics play an additional role in coupled models (Kang et al., 2019). Here we show that the same processes contribute to the SST response in the tropical South Atlantic to the observed SO cooling.

Unlike the idealized SO studies cited above, which examined the equilibrium response to large amplitude perturbations, we investigate the transient response to a much smaller and realistic perturbation, namely the observed cooling of SO SSTs in recent decades. In particular, we address the following questions. Does observed SO cooling produce a robust, remote climate response that extends into the tropics? If so, what is the nature of the response pattern and its underlying mechanisms? To what extent is the observed expansion of Antarctic sea ice controlled by SO SST cooling? To probe these questions, we apply a "pacemaker" experimental protocol (Kosaka & Xie, 2013) by nudging SO SST anomalies in a fully coupled global climate model to follow the observed evolution over the period 1979–2013. This protocol has previously been applied to the tropical Pacific to study the origins of the global surface warming hiatus (e.g., Kosaka & Xie, 2013; Deser, Guo, & Lehner, 2017), as well as teleconnections from ENSO and the tropical lobe of the PDO (i.e., Schneider & Deser, 2018; Deser, Simpson, et al., 2017), and to the North Atlantic for assessing the global impact of observed Atlantic multidecadal variability (i.e., Ruprich-Robert et al., 2016). To the best of our knowledge, we are the first to apply the "pacemaker" protocol to investigate the influence of observed SO SST evolution on the the global coupled climate system. The effects of observed SO cooling are compared with those from observed tropical Pacific SST changes based on the Pacific Pacemaker simulations (TPACE, Deser, Guo, & Lehner, 2017), as well as the radiatively-forced response derived from the Community Earth System Model version 1 (CESM1) Large Ensemble Project (LENS, Kay et al., 2015); note that all three sets of simulations employ the identical model version for direct comparison. We describe our experimental design and data in section 2, followed by results in section 3. We end with summary and discussion in section 4.

2 Model and Experimental Design

We conduct a 20-member ensemble of SO "Pacemaker" Experiments (SOPACE) with CESM1.1.2 at 1° horizontal resolution, the same version used for LENS (Kay et al., 2015). The methodology follows Kosaka and Xie (2013) (also detailed in Deser, Guo, and Lehner (2017)). Briefly, SST anomalies (as opposed to absolute SSTs to avoid the model's mean state warm biases in the SO, C. Wang et al., 2014) at each grid box over the SO are nudged to the observed evolution of SST anomalies from 1975 to 2016 taken from the NOAA Extended Reconstruction Sea Surface Temperature version 3b (ERSSTv3b) data set (Smith et al., 2008). The nudging region covers ocean grids south of 40°S, with a linearly tapering buffer zone from 35°S to 40°S. In regions with LENS climatological sea ice cover, SST is nudged to the melting temperature of -1.8°C. The nudging timescale is 2 days for the model's 10-m deep ocean surface layer, which is equivalent to the 10-day timescale for a 50-m deep mixed layer used in Kosaka and Xie (2013). Outside of the nudging region, the model's coupled climate system evolves freely. All simulations are subject to historical radiative forcing before 2005 and the RCP8.5 scenario thereafter, following the CMIP5 protocols (Taylor et al., 2011). All SOPACE members are initialized from the first member of LENS on 1 Jan 1975, with a random initial atmospheric temperature perturbation of $\mathcal{O}(10^{-14})$ K to create ensemble spread. The surface heat flux forcing used to nudge the model's SST anomalies shows significant spatial and temporal variations over the SO (not shown). The total energy perturbation in SOPACE is approximately -0.1 PW, which is much less than that used in idealized experiments cited earlier, for example, -0.8 PW in Kang et al. (2019).

We also analyze the LENS and a 20-member ensemble of the TPACE, also conducted with CESM1.1.2 (Deser, Guo, & Lehner, 2017; Schneider & Deser, 2018). TPACE shares the same experimental design as SOPACE, but with nudging in the tropical eastern Pacific (15°N–15°S; 80°–180°W) over the period 1920–2013. LENS consists of 40 members that extend from 1920 to 2100, and shares the same historical and RCP8.5 forcing with SOPACE and TPACE, but has no nudging toward observations. The LENS ensemble mean (EM) is used to define the model's response to external forcing, and the spread about the EM defines the model's internal variability. Observational data sets are described in supporting information.

3 Results

3.1 SST Trends

We examine trends over the period 1979–2013 when the SO surface cooled, consistent with Schneider and Deser (2018). Figure 1a–d show the observed and EM SST trends from LENS, TPACE, and SOPACE. Over the Pacific, observations show a large-scale pattern reminiscent of the negative phase of the PDO and IPO, with warming in the west and cooling in the east. In the Atlantic, positive SST trends in the sub-polar gyre and the tropical North Atlantic resemble the positive phase of the AMO. The Indian Ocean shows near-uniform surface warming. The SO cools overall, except for the Indian sector, with the strongest cooling in the Pacific sector north of the Amundsen and Bellingshausen Sea (Figure 1a).

The LENS-EM SST trend pattern, which represents the model's radiatively-forced response, differs considerably from observations (Figure 1b). LENS-EM shows warming around 0.1–0.2 K/decade over most of the global ocean, with the notable exception of the subpolar North Atlantic, which cools as a result of a slowdown of the Atlantic Meridional Overturning Circulation (AMOC, Drijfhout et al., 2012). Enhanced equatorial warming occurs in the Pacific and Atlantic, while muted warming is found in southeast and northeast subtropical Pacific. Unlike observations, positive SST trends are evident throughout the SO (except along the Antarctic coastline), with enhanced warming in the Atlantic sector. This leads to the interpretation based on LENS that the recent observed SO cooling is internally generated; however, potential biases in the model's forced response and/or the lack of an interactive Antarctic ice sheet in CESM1 may affect this interpretation (e.g., Bronselaer et al., 2018). Unlike LENS-EM, TPACE-EM shows a negative PDO/IPO pattern that bears a close resemblance to observations (Figure 1c). However, the observed cooling over the SO is generally not simulated in TPACE-EM, except in the eastern Pacific sector where weak cooling occurs. This indicates that while the tropical Pacific has some influence on the SO, it is not large enough to overwhelm the radiatively-forced response (see also Schneider & Deser, 2018). In the tropical Atlantic, SST trends in TPACE-EM are generally of opposite sign compared to observations. Unlike TPACE-EM, SOPACE-EM shows a realistic pattern of SST trends in the tropical Atlantic, with greater warming in the north compared to the south, although the amplitude of this dipole is weaker than observed (Figure 1d). More importantly, the pattern of SST trends in the tropical Atlantic in SOPACE-EM differs from the radiatively-forced response (LENS-EM), indicating a significant influence of SO SSTs in this region. SOPACE-EM also shows greater cooling in the southeast subtropical Pacific compared to LENS-EM.

To isolate the non-radiatively-forced responses in TPACE-EM and SOPACE-EM, we subtract the LENS-EM trends. We term this residual trend the internally-forced response (denoted "TPACE-internal" and "SOPACE-internal", Figure 1e and 1f), as it refers to the model's response to an imposed "forcing" that is internally-generated, as opposed to the externally-generated radiative forcing. In both TPACE-internal and SOPACE-internal, the SST trends are negative over much of the globe. In TPACE-internal, the negative PDO/IPO pattern is generally preserved, and we see significant cooling in the tropical North Atlantic, leading to a north-south tropical Atlantic SST gradient that is opposite to observations. On the other hand, in SOPACE-internal, significant cooling is found in the tropical South Atlantic with maximum amplitude along the west coast of Africa.

In the North Atlantic, SOPACE-internal shows cooling in the subpolar gyre, co-located with the radiatively-forced "warming hole" in LENS-EM. Because of the connection between AMOC and the subpolar gyre SST (Rahmstorf et al., 2015), this cooling suggests that the observed SO cooling may also contribute to AMOC slowdown. Although the median of the SOPACE ensemble AMOC trend is lower than that of the LENS ensemble (Figure S2), but not significantly so (p value $=$ 0.3). Furthermore, caution is needed in interpreting the deep ocean circulation response in SOPACE due to the experimental protocol: SOPACE-internal exhibits significant subsurface cooling in the SO down to $\sim$300 m depth (not shown), contrary to the observed subsurface warming and positive trend in SO heat uptake (Armour et al., 2016; Tung & Chen, 2018).

3.2 Tropical South Atlantic Response

The most significant remote response in SOPACE-internal is the SST cooling in the tropical South Atlantic (Figure 1f and 2a). This cooling extends all the way to the equator, with maximum amplitude in the tropical southeastern Atlantic. As mentioned earlier, this SO-induced cooling of the tropical South Atlantic brings the pattern of SST trends over the entire tropical Atlantic in SOPACE-EM into closer alignment with observations. In particular, there is a positive north-south gradient in both observations and SOPACE-EM, opposite to that in TPACE-EM and distinct from LENS-EM (Figure 1). To explore the robustness of this feature, we show the ensemble distribution of SST trends averaged over the tropical South Atlantic (TSA: 10–30°S, 20°W–10°E; gray box in Figure 1f) in LENS, TPACE, and SOPACE (Figure 1g). The observed TSA trend is weakly positive at 0.053 K/decade (horizontal gray line in Figure 1g), and lies within the middle 50% of the SOPACE distribution, but only within the bottom 10% of LENS and bottom 25% of TPACE. In addition, the TSA trend spread is half as large in SOPACE compared to LENS and TPACE. In summary, it is more likely for SOPACE members to have a TSA trend that is consistent with observations than it is for LENS or TPACE members, and the distribution of TSA trend in SOPACE is more constrained than those in either LENS or TPACE.

We have also compared the basin-wide patterns of Atlantic SST trends between observations and the model ensembles over the domain 20°N–40°S, 70°W–15°E (gray box in Figure 1a). The pattern correlation (r) with observations is considerably higher for SOPACE ($r(\text{obs}, \text{EM})_{\text{SOPACE}} = 0.64$) than for either LENS ($r(\text{obs}, \text{EM})_{\text{LENS}} = 0.20$) or TPACE ($r(\text{obs}, \text{EM})_{\text{TPACE}} = -0.28$), consistent with visual impression from Figure 1 (green stars in Figure 1h). This suggests that the internally-forced response to observed SO cooling makes a substantial contribution to the spatial pattern of observed SST trends over the broad Atlantic region (and that the radiatively-forced response cannot sufficiently explain the observed SST trend pattern over the Atlantic).

In order to better quantify the spread due to internal variability, we also computed the pattern correlation between each ensemble member i and the EM of each experiment (denoted $r(i, \text{EM})$). The range of $r(i, \text{EM})_{\text{SOPACE}}$ spans from 0.41-0.81, with $r(\text{obs}, \text{EM})_{\text{SOPACE}}$ lying in the center of the distribution. This indicates that the inclusion of observed internal SO cooling results in a more realistic pattern of simulated SST trends over the broad (20°N–40°S) Atlantic domain. Moreover, the observed SST trend pattern in this region resembles the simulated response to SO cooling. The distribution of $r(i, \text{EM})_{\text{TPACE}}$, on the other hand, does not encompass the negative $r(\text{obs}, \text{EM})_{\text{TPACE}}$, further emphasizing the inability of the observed tropical eastern Pacific cooling to produce the observed pattern of Atlantic SST trends (Figure 1h). While the distribution of $r(i, \text{EM})_{\text{LENS}}$ also encompasses the observed pattern correlation, $r(\text{obs}, \text{EM})_{\text{LENS}}$ is much lower than $r(\text{obs}, \text{EM})_{\text{SOPACE}}$. Furthermore, in the LENS ensemble, the influence of the model's internal SO SST trends on the Atlantic pattern correlations cannot be isolated.

3.3 Ocean Mixed Layer Heat Budget Analysis

What processes contribute to the remote Atlantic SST response in SOPACE? To answer this question, we analyze the heat budget of the upper ocean mixed layer following Xie et al. (2010),

$$\rho c_p H \frac{\partial T_s}{\partial t} = F_{\text{SW}} + F_{\text{LW}} + SH + LH + O, \tag{1}$$

where ρ is the density of ocean, c_p is the specific heat of ocean, H is the ocean mixed-layer depth, T_s is the mixed-layer temperature. Hence the left-hand side (LHS) represents the mixed-layer heat storage term. The right-hand side (RHS) consists of net surface shortwave (F_{SW}) and longwave (F_{LW}) fluxes, sensible (SH) and latent (LH) heat fluxes, and heat flux due to ocean dynamics (O). Our convention is that positive values on the RHS warm T_s and vice versa. We compute the ensemble-mean trend (1979-2013) of each term in Equation 1 for SOPACE-internal in order to isolate the forced response to the internal component of observed SO SST trends. Maps of the trends in each quantity (denoted by the superscript t, e.g., F^t_{SW}) are shown in Figure S4 for the tropical eastern Pacific and Atlantic domain. Heat storage trends are negligible (Figure S4b), indicating that the trends of the RHS terms of Equation 1 are in quasi-equilibrium. A similar result was shown by Cook et al. (2018) based on ocean reanalysis products. This allows us to compute O^t as a residual term (Equation S2).

The dependency of latent heat flux on SST allows us to rewrite Equation 1 as a diagnostic equation of the SST trend T^t_s, following Jia and Wu (2013) and Hwang et al. (2017) (see derivation in supporting information):

$$T^t_s = T^t_{\mathrm{SW}} + T^t_{\mathrm{LW}} + T^t_{\mathrm{SH}} + T^t_{\mathrm{O}} + T^t_{\mathrm{LH,w}} + T^t_{\mathrm{LH,RH}} + T^t_{\mathrm{LH},\Delta\mathrm{T}}. \tag{2}$$

The RHS in Equation 2 represents the contributions to SST trend from F_{SW}, F_{SW}, SH, O, and LH. The latent heat term can be further broken down into contributions from trends in near-surface wind $T^t_{\mathrm{LH,w}}$, near-surface relative humidity $T^t_{\mathrm{LH,RH}}$, and air-sea temperature gradient $T^t_{\mathrm{LH},\Delta\mathrm{T}}$. The sum of the terms on the RHS of Equation 2 (Figure 2a) closely approximates the actual T^t_s (Figure 1f), validating our methodology. The major terms contributing to cooling trends in both basins include T^t_{SW} (due to increased cloud liquid water, Figure 2b), T^t_{O} (largely due to Ekman advection, Figure 2e), and $T^t_{\mathrm{LH,w}}$ (due to strengthened trade winds, Figure 2f).

In the Atlantic, the contribution from F_{SW} is centered at the coastal stratocumulus region between 10–15°S. A positive trend in liquid water path is expected as the SST cools and strengthens the cloud top temperature inversion. The equatorial Atlantic cooling is dominated by the WES feedback, where there is a strengthening of the southeasterly trade winds, which enhances evaporative cooling. At 25°S, the strengthened winds not only cool the SST via WES feedback, but also via Ekman advection (Figure S6). In the Eastern Pacific, F_{SW} plays a more dominant role in cooling the SST than in the Atlantic, due to a weaker near-surface wind response and associated LH. To summarize, the pattern of the negative T_s^t is caused by the sum of contributing terms instead of dominated by a single heat flux trend.

3.4 Antarctic Sea Ice Trends

Observational evidence suggests that multidecadal SST and wind variability over the SO plays an essential role in governing the pattern of Antarctic sea ice trends (Fan et al., 2014; Armour & Bitz, 2015). Can SOPACE reproduce the observed trends in Antarctic sea ice? The observed Antarctic sea ice extent (SIE) trend during this period is 0.23×10^6 km^2 per decade, which is drastically different from the radiatively-forced SIE trend of -0.36×10^6 km^2 per decade in LENS-EM and -0.30×10^6 km^2 per decade in TPACE-EM (Figure 3a). In contrast, SOPACE-EM shows an Antarctic SIE trend of -0.040×10^6 km^2 per decade, a rate that is an order of magnitude slower than in LENS-EM and TPACE-EM. Furthermore, 40% of SOPACE ensemble members show a positive SIE trend, although none is as large as observed (the largest trend in SOPACE is 0.084×10^6 km^2 per decade; Figure 3a). The significant differences between Antarctic SIE trends in SOPACE-EM, LENS-EM, and TPACE-EM indicate that observed SO SST cooling plays an import role in influencing Antarctic SIE, though it is not the only factor.

In addition to differences in the total SIE trend, there are significant differences in the patterns of sea ice concentration (SIC) trends among observations and the model ensembles. The observed SIC shows positive trends over most of the SO, except for the West Antarctic coastline and north of the Weddell Sea (Figure 3c). LENS-EM shows a nearly zonally-symmetric negative SIC trend pattern (Figure 3d), similar to that in TPACE-EM although with weaker magnitude in the Atlantic and Pacific sectors (Figure 3e; see also Figure 3g). On the other hand, SIC trends in SOPACE-EM show a mixture of positive and negative values, with ice gain in the Bellingshausen Sea and ice loss in the Weddell Sea (Figure 3f). Indeed, the imposed SST cooling in the SO leads to a marked Antarctic-wide expansion of sea ice relative to the radiatively-forced response (Figure 3h).

Although observed SO cooling produces an Antarctic-wide increase in SIC, when combined with the radiatively-forced response, the SIC trend pattern in SOPACE-EM differs from observations. For example, SOPACE-EM produces sea ice gain in the Bellingshausen Sea and Drake Passage but ice loss in the Weddell Sea and Ross Sea, opposite to observations (Figure 3f and 3c). At first glance, this seems to contradict the observational evidence that positive SIC trends are associated with SST cooling, and vice versa. However, observations also suggest that near-surface winds can drive thermodynamic sea ice changes via temperature advection. In general, anomalous northerly winds contribute to SST increase and sea ice loss via warm air advection, while anomalous southerlies correspond to opposite conditions (Fan et al., 2014). Indeed, north of the Weddell Sea and Antarctic Peninsula, ERA-5 shows northerly near-surface winds that are generally associated with warm-air advection and sea ice loss. In the Ross Sea, southerly winds are co-located with positive SIC trends (Figure 3c). In the Amundsen Sea, southerly wind trends are associated with negative sea ice trends along the coast, consistent with the finding that ice advection driven by local winds dominates the sea ice loss there (Holland & Kwok, 2012). The near-surface wind trends in SOPACE-EM display significant pattern differences from observations, especially in the Amundsen Sea and the Ross Sea (Figure 3f), which partially explain the differences in regional SIC trends between SOPACE-EM and observations. We note, however, that the highest pattern correlation between SIC trends in any single member of SOPACE and observations is only 0.16. Furthermore, the range of $r(i, \mathrm{EM})_{\mathrm{SOPACE}}$ (0.38–0.91) does not encompass $r(obs, \mathrm{EM})_{\mathrm{SOPACE}} = -0.11$ (Figure 3b). Thus, our results suggest that specifying the observed SO SST trends in CESM1 does not guarantee a match between the observed and simulated response of Antarctic SIC trends, and exposes model biases in both the radiatively-forced component as well as patterns of internally-generated SIC trends in SOPACE. Processes such as ocean-ice shelf interaction are absent in CESM1, potentailly contributing to biases, e.g., in the Weddell Sea (Park & Latif, 2019).

4 Summary and Discussion

We have examined the remote impact of observed SO SST cooling during 1979–2013 in CESM1 using a 20-member initial-condition ensemble in which SST anomalies over the SO are nudged to the observed monthly evolution (SOPACE). The results are compared to the 20-member TPACE, where the same protocol was applied to SSTs in the tropical eastern Pacific, as well as the freely evolving 40-member LENS. The forced response in each experiment is estimated by the EM.

The most significant influence of the observed SO cooling is found in the tropical South Atlantic. In this region, the observed SO cooling leads to a significant reduction in the radiatively-forced warming trend, enhancing the north-south gradient in tropical Atlantic SST trends. The muted tropical Atlantic warming south of the equator compared to the north in SOPACE-EM resembles the observed SST trend pattern, which neither TPACE-EM nor LENS-EM captures. Indeed, TPACE-EM shows an opposite trend in the tropical Atlantic SST gradient. Furthermore, it is more likely for SOPACE members to have realistic tropical South Atlantic SST trends than either LENS or TPACE members. The SOPACE ensemble also has a realistic depiction of the SO cooling's influence on the broader tropical Atlantic SST trend pattern, unlike TPACE. The tropical South Atlantic response suggests an important role the SO SST plays on decadal time scales, consistent with previous findings (Cabré et al., 2017).

A mixed layer heat budget analysis of the tropical South Atlantic region shows that increased low-level cloud amount and enhanced trade winds contribute to reducing SSTs via shortwave radiative flux and the WES-feedback mechanism, respectively. Ekman advection also contributes to SST cooling along the African coast where strong climatological SST gradients exist. The observed trends of low-level cloud amount are significantly positive over the southeastern Atlantic and Pacific during 1984–2009, consistent with our findings based on SOPACE-internal (Seethala et al., 2015). Multilinear regression analysis suggests that strengthened inversion stability is the dominant cloud-controlling factor for the observed positive low-cloud amount trends. The processes that contribute to the SO induced cooling are consistent with the idealized studies (Hwang et al., 2017; Kang et al., 2019), although the WES feedback is much weaker in the tropical eastern Pacific in SOPACE-internal.

Antarctic SIE has increased during 1979–2013, opposite to the radiatively-forced decrease in LENS-EM. While the SIE trend in TPACE-EM is similar to that in LENS-EM, SIE trend in SOPACE-EM is near zero, and 40% of SOPACE ensemble members show positive SIE trends although none as large as observed. Furthermore, the observed SO cooling leads to Antarctic-wide positive SIC trends in SOPACE-internal, but because of differences in near-surface wind trends, the spatial pattern of the simulated SIC trends differs from observations. The low pattern correlations between observed SIC trends and those in the individual members of SOPACE, and the negative pattern correlation between observed SIC trends and those in SOPACE-EM (which lies outside the distribution of pattern correlations between individual members of SOPACE and SOPACE-EM), indicates a likely bias in the amplitude and pattern of the model's radiatively-forced SIC trends.

Our results may have implications for understanding the future trajectory of Antarctic sea ice and tropical South Atlantic SSTs. Indeed, SSTs have recently warmed in the SO while Antarctic SIE reached record low values in 2017 (Parkinson, 2019; Meehl et al., 2019). If this SO SST warming trend continues, the tropical South Atlantic may experience accelerated warming due to the combined influence from SO SSTs and increasing greenhouse gas concentrations. Future work is needed to investigate the predictability of these impacts relative to other sources of internal variability in the coming decades.

Acknowledgments

We thank the reviewers for their constructive comments, and Nan Rosenbloom for helping with the pacemaker experimental setup. X.Z. is supported by an Advanced Study Program postdoctoral fellowship from the National Center for Atmospheric Research and the National Science Foundation Office of Polar Programs. This material is based upon work supported by the National Center for Atmospheric Research, which is a major facility sponsored by the National Science Foundation under Cooperative Agreement No. 1852977. We would like to acknowledge high-performance computing support from Cheyenne (doi:10.5065/D6RX99HX) provided by NCAR's Computational and Information Systems Laboratory, sponsored by the National Science Foundation. Data are available at https://doi.org/10.5065/arn2-5j02.

References

Alexander, M. A., Bladé, I., Newman, M., Lanzante, J. R., Lau, N.-C., & Scott, J. D. (2002). The atmospheric bridge: the influence of ENSO teleconnections on air–sea interaction over the global oceans. *Journal of Climate*, *15*(16), 2205–2231. doi: 10.1175/1520-0442(2002)015⟨2205:TABTIO⟩2.0.CO;2

Alexander, M. A., Vimont, D. J., Chang, P., & Scott, J. D. (2010). The impact of extratropical atmospheric variability on ENSO: testing the seasonal footprinting mechanism using coupled model experiments. *Journal of Climate*, *23*(11), 2885–2901. doi: 10.1175/2010JCLI3205.1

Amaya, D. J., Kosaka, Y., Zhou, W., Zhang, Y., Xie, S.-P., & Miller, A. J. (2019). The North Pacific pacemaker effect on historical ENSO and its mechanisms.

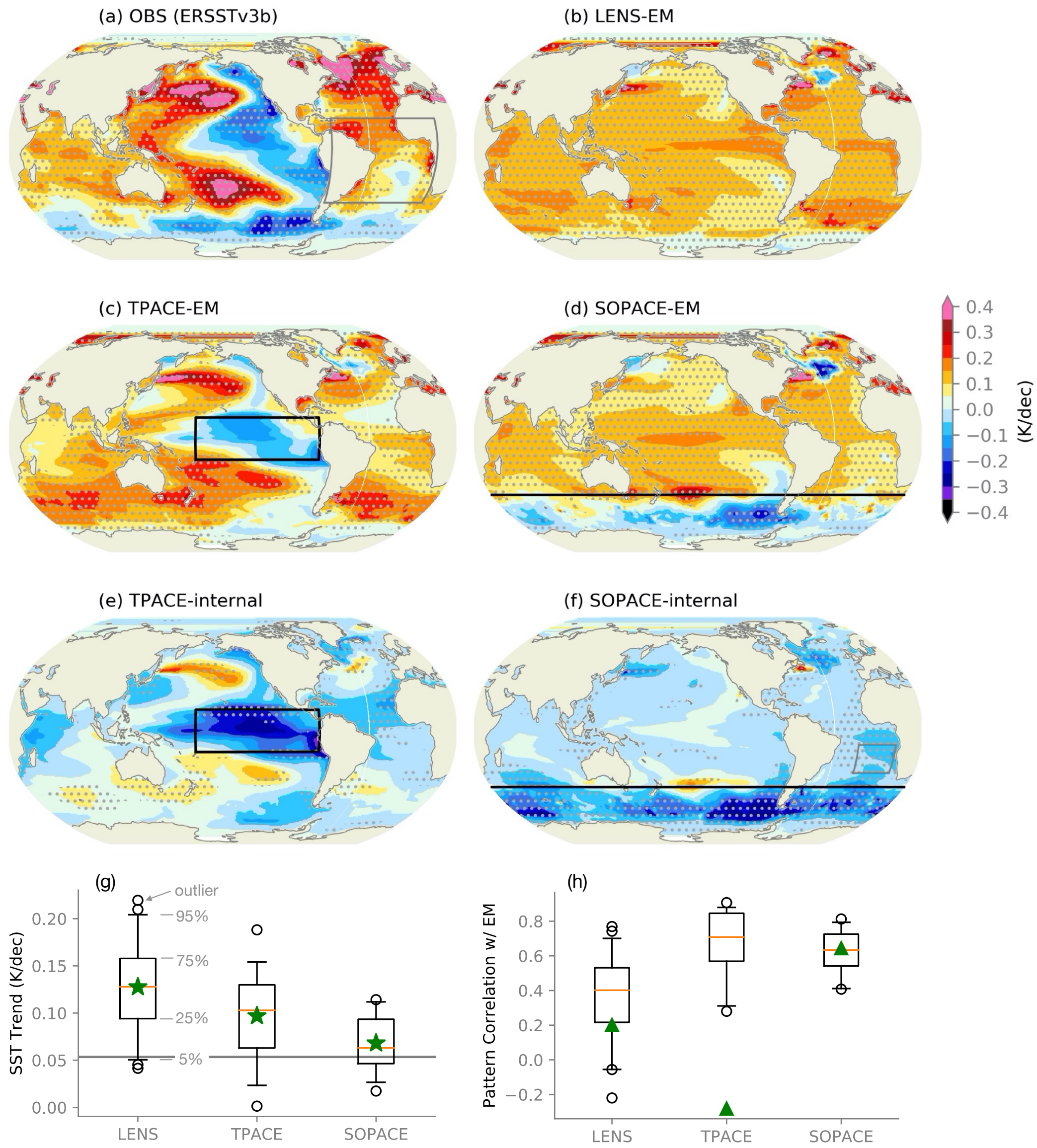

Figure 1. Monthly SST trends over 1979–2013 for (a) ERSSTv3b, (b) LENS-EM, (c) TPACE-EM, (d) SOPACE-EM, (e) TPACE-internal, and (f) SOPACE-internal. Stippling indicates local trend that is significant at or above 95% level. Black lines outline the SST nudging domain. (g) Box-and-whisker plot of SST trends averaged over the tropical South Atlantic (gray box in (f)) for each model ensemble. Green stars show the EM values. Orange lines show the median values. Gray horizontal line shows the observed value. (h) Same as (g) but for pattern correlations of SST trends with EM $r(i, \mathrm{EM})$ over the broader Atlantic region (gray box in (a)). Green triangles show $r(\mathrm{obs}, \mathrm{EM})$.

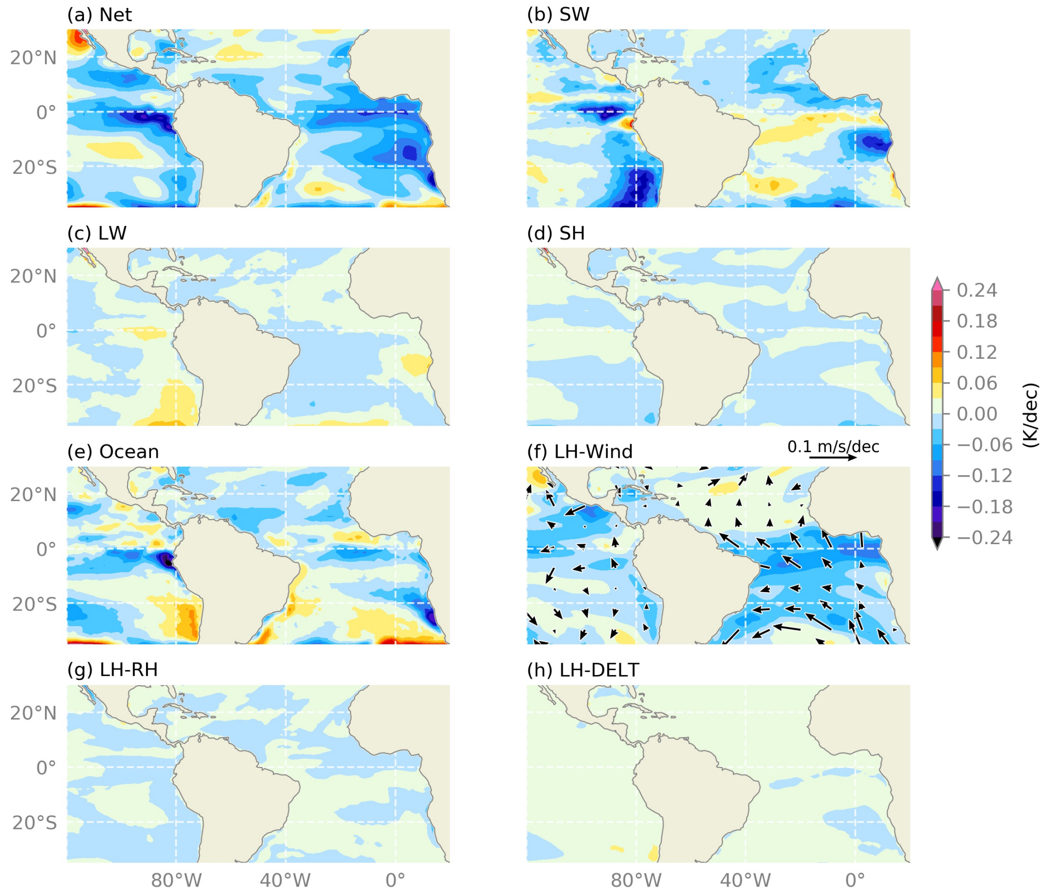

Figure 2. SST trend decomposition based on Equation 2 using monthly trends during 1979–2013 from SOPACE-internal over the tropical eastern Pacific and Atlantic: (a) net T_s^t, (b) T_{SW}^t, (c) T_{LW}^t, (d) T_{SH}^t, (e) T_{O}^t, (f) $T_{\mathrm{LH,W}}^t$ with near-surface wind trends overlaid (vectors), (g) $T_{\mathrm{LH,RH}}^t$, and (h) $T_{\mathrm{LH,\Delta T}}^t$.

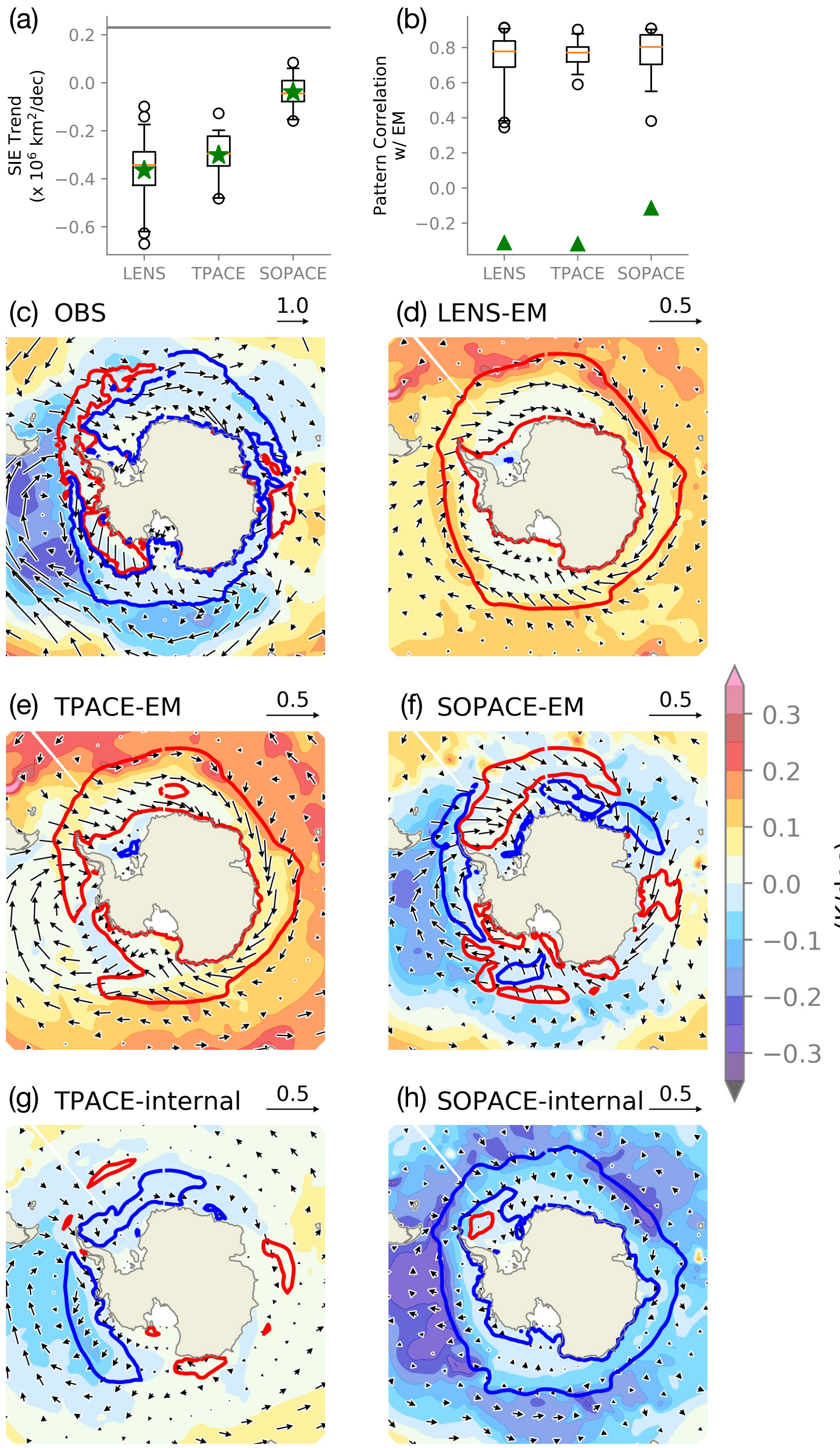

Figure 3. (a) Box-and-whisker plot of Antarctic SIE trends for each model ensemble. Green stars show the EM values. Orange lines show the median values. Gray horizontal line shows the observed value. (b) Same as (a) but for pattern correlations of SIC trends with EM $r(i, \mathrm{EM})$ over 50–80°S. Green triangles show $r(\mathrm{obs}, \mathrm{EM})$. Monthly SST (colors), SIC (contours), and near-surface wind (vectors, m/s/decade) trends over 1979–2013 for (a) ERSSTv3b, (b) LENS-EM, (c) TPACE-EM, (d) SOPACE-EM, (e) TPACE-internal, and (f) SOPACE-internal. Blue (positive) and red (negative) contours outline regions with SIC trend magnitudes greater than 0.5%/decade.

Journal of Climate, *32*(22), 7643–7661. doi: 10.1175/JCLI-D-19-0040.1

Armour, K. C., & Bitz, C. M. (2015). Observed and projected trends in Antarctic sea ice. *US CLIVAR Var*, *13*.

Armour, K. C., Marshall, J., Scott, J. R., Donohoe, A., & Newsom, E. R. (2016). Southern Ocean warming delayed by circumpolar upwelling and equatorward transport. *Nature Geoscience*, *9*(7), 549–554. doi: 10.1038/ngeo2731

Bintanja, R., van Oldenborgh, G. J., Drijfhout, S. S., Wouters, B., & Katsman, C. A. (2013). Important role for ocean warming and increased ice-shelf melt in Antarctic sea-ice expansion. *Nature Geoscience*, *6*(5), 376–379. doi: 10.1038/ngeo1767

Bronselaer, B., Winton, M., Griffies, S. M., Hurlin, W. J., Rodgers, K. B., Sergienko, O. V., … Russell, J. L. (2018). Change in future climate due to Antarctic meltwater. *Nature*, *564*(7734), 53–58. doi: 10.1038/s41586-018-0712-z

Cabré, A., Marinov, I., & Gnanadesikan, A. (2017). Global atmospheric teleconnections and multidecadal climate oscillations driven by Southern Ocean convection. *Journal of Climate*, *30*(20), 8107–8126. doi: 10.1175/JCLI-D-16-0741.1

Cook, K. H., Vizy, E. K., & Sun, X. (2018). Multidecadal-scale adjustment of the ocean mixed layer heat budget in the tropics: examining ocean reanalyses. *Climate Dynamics*, *50*(5), 1513–1532. doi: 10.1007/s00382-017-3703-0

Deser, C., Guo, R., & Lehner, F. (2017). The relative contributions of tropical Pacific sea surface temperatures and atmospheric internal variability to the recent global warming hiatus. *Geophysical Research Letters*, *44*(15), 7945–7954. doi: 10.1002/2017GL074273

Deser, C., Phillips, A. S., & Hurrell, J. W. (2004). Pacific interdecadal climate variability: linkages between the Tropics and the North Pacific during boreal winter since 1900. *Journal of Climate*, *17*(16), 3109–3124. doi: 10.1175/1520-0442(2004)017⟨3109:PICVLB⟩2.0.CO;2

Deser, C., Simpson, I. R., McKinnon, K. A., & Phillips, A. S. (2017). The Northern Hemisphere extratropical atmospheric circulation response to ENSO: How well do we know it and how do we evaluate models accordingly? *Journal of Climate*, *30*(13), 5059–5082. doi: 10.1175/JCLI-D-16-0844.1

Deser, C., Tomas, R. A., & Sun, L. (2015). The role of ocean–atmosphere coupling in the zonal-mean atmospheric response to Arctic sea ice loss. *Journal of Cli-*

mate, *28*(6), 2168–2186. doi: 10.1175/JCLI-D-14-00325.1

Drijfhout, S., van Oldenborgh, G. J., & Cimatoribus, A. (2012). Is a decline of AMOC causing the warming hole above the North Atlantic in observed and modeled warming patterns? *Journal of Climate*, *25*(24), 8373–8379. doi: 10.1175/JCLI-D-12-00490.1

Enfield, D. B., Mestas-Nuñez, A. M., & Trimble, P. J. (2001). The Atlantic Multidecadal Oscillation and its relation to rainfall and river flows in the continental U.S. *Geophysical Research Letters*, *28*(10), 2077–2080. doi: 10.1029/2000GL012745

England, M. R., Polvani, L. M., Sun, L., & Deser, C. (2020). Tropical climate responses to projected Arctic and Antarctic sea-ice loss. *Nature Geoscience*, 1–7. doi: 10.1038/s41561-020-0546-9

Fan, T., Deser, C., & Schneider, D. P. (2014). Recent Antarctic sea ice trends in the context of Southern Ocean surface climate variations since 1950. *Geophysical Research Letters*, *41*(7), 2419–2426. doi: 10.1002/2014GL059239

Ferreira, D., Marshall, J., Bitz, C. M., Solomon, S., & Plumb, A. (2014). Antarctic ocean and sea ice response to ozone depletion: a two-time-scale problem. *Journal of Climate*, *28*(3), 1206–1226. doi: 10.1175/JCLI-D-14-00313.1

Hersbach, H., Bell, W., Berrisford, P., Horányi, A., Muñoz-Sabater, J., Nicolas, J., … Dee, D. (2019). Global reanalysis: goodbye ERA-Interim, hello ERA5. *ECMWF Newsletter*, *159*, 17–24. doi: 10.21957/vf291hehd7

Holland, P. R., & Kwok, R. (2012). Wind-driven trends in Antarctic sea-ice drift. *Nature Geoscience*, *5*(12), 872–875. doi: 10.1038/ngeo1627

Huang, B., Thorne, P. W., Banzon, V. F., Boyer, T., Chepurin, G., Lawrimore, J. H., … Zhang, H.-M. (2017). Extended Reconstructed Sea Surface Temperature, Version 5 (ERSSTv5): upgrades, validations, and intercomparisons. *Journal of Climate*, *30*(20), 8179–8205. doi: 10.1175/JCLI-D-16-0836.1

Hwang, Y.-T., Xie, S.-P., Deser, C., & Kang, S. M. (2017). Connecting tropical climate change with Southern Ocean heat uptake. *Geophysical Research Letters*, *44*(18), 9449–9457. doi: 10.1002/2017GL074972

Ishii, M., Shouji, A., Sugimoto, S., & Matsumoto, T. (2005). Objective analyses of sea-surface temperature and marine meteorological variables for the 20th century using ICOADS and the Kobe Collection. *International Journal of*

Climatology, *25*(7), 865–879. doi: 10.1002/joc.1169

Jia, F., & Wu, L. (2013). A study of response of the Equatorial Pacific SST to doubled-CO2 forcing in the coupled CAM–1.5-layer reduced-gravity ocean model. *Journal of Physical Oceanography*, *43*(7), 1288–1300. doi: 10.1175/JPO-D-12-0144.1

Kang, S. M., Hawcroft, M., Xiang, B., Hwang, Y.-T., Cazes, G., Codron, F., ... Yu, S. (2019). ETIN-MIP Extratropical-Tropical Interaction Model Intercomparison Project – protocol and initial results. *Bulletin of the American Meteorological Society*. doi: 10.1175/BAMS-D-18-0301.1

Kay, J. E., Deser, C., Phillips, A., Mai, A., Hannay, C., Strand, G., ... Vertenstein, M. (2015). The Community Earth System Model (CESM) large ensemble project: a community resource for studying climate change in the presence of internal climate variability. *Bulletin of the American Meteorological Society*, *96*(8), 1333–1349. doi: 10.1175/BAMS-D-13-00255.1

Kerr, R. A. (2000). A North Atlantic climate pacemaker for the centuries. *Science*, *288*(5473), 1984–1985. doi: 10.1126/science.288.5473.1984

Kosaka, Y., & Xie, S.-P. (2013). Recent global-warming hiatus tied to equatorial Pacific surface cooling. *Nature*, *501*(7467), 403–407. doi: 10.1038/nature12534

Kostov, Y., Ferreira, D., Armour, K. C., & Marshall, J. (2018). Contributions of greenhouse gas forcing and the Southern Annular Mode to historical Southern Ocean surface temperature trends. *Geophysical Research Letters*, *45*(2), 1086–1097. doi: 10.1002/2017GL074964

Latif, M., Martin, T., & Park, W. (2013). Southern Ocean sector centennial climate variability and recent decadal trends. *Journal of Climate*, *26*(19), 7767–7782. doi: 10.1175/JCLI-D-12-00281.1

Liguori, G., & Di Lorenzo, E. (2019). Separating the North and South Pacific Meridional Modes contributions to ENSO and tropical decadal variability. *Geophysical Research Letters*, *46*(2), 906–915. doi: 10.1029/2018GL080320

Mantua, N. J., Hare, S. R., Zhang, Y., Wallace, J. M., & Francis, R. C. (1997). A Pacific interdecadal climate oscillation with impacts on salmon production. *Bulletin of the American Meteorological Society*, *78*(6), 1069–1080. doi: 10.1175/1520-0477(1997)078⟨1069:APICOW⟩2.0.CO;2

Mechoso, C. R., Losada, T., Koseki, S., Mohino-Harris, E., Keenlyside, N., Castaño-

Tierno, A., … Toniazzo, T. (2016). Can reducing the incoming energy flux over the Southern Ocean in a CGCM improve its simulation of tropical climate? *Geophysical Research Letters*, *43*(20), 11,057–11,063. doi: 10.1002/2016GL071150

Meehl, G. A., Arblaster, J. M., Chung, C. T. Y., Holland, M. M., DuVivier, A., Thompson, L., … Bitz, C. M. (2019). Sustained ocean changes contributed to sudden Antarctic sea ice retreat in late 2016. *Nature Communications*, *10*(1), 1–9. doi: 10.1038/s41467-018-07865-9

Newman, M., Alexander, M. A., Ault, T. R., Cobb, K. M., Deser, C., Di Lorenzo, E., … Smith, C. A. (2016). The Pacific Decadal Oscillation, revisited. *Journal of Climate*, *29*(12), 4399–4427. doi: 10.1175/JCLI-D-15-0508.1

Park, W., & Latif, M. (2019). Ensemble global warming simulations with idealized Antarctic meltwater input. *Climate Dynamics*, *52*(5-6), 3223–3239. doi: 10.1007/s00382-018-4319-8

Parkinson, C. L. (2019). A 40-y record reveals gradual Antarctic sea ice increases followed by decreases at rates far exceeding the rates seen in the Arctic. *Proceedings of the National Academy of Sciences*, *116*(29), 14414–14423. doi: 10.1073/pnas.1906556116

Peng, G., Meier, W. N., Scott, D. J., & Savoie, M. H. (2013). A long-term and reproducible passive microwave sea ice concentration data record for climate studies and monitoring. *Earth System Science Data*, *5*(2), 311–318. doi: 10.5194/essd-5-311-2013

Power, S., Casey, T., Folland, C., Colman, A., & Mehta, V. (1999). Inter-decadal modulation of the impact of ENSO on Australia. *Climate Dynamics*, *15*(5), 319–324. doi: 10.1007/s003820050284

Rahmstorf, S., Box, J. E., Feulner, G., Mann, M. E., Robinson, A., Rutherford, S., & Schaffernicht, E. J. (2015). Exceptional twentieth-century slowdown in Atlantic Ocean overturning circulation. *Nature Climate Change*, *5*(5), 475–480. doi: 10.1038/nclimate2554

Rayner, N. A., Parker, D. E., Horton, E. B., Folland, C. K., Alexander, L. V., Rowell, D. P., … Kaplan, A. (2003). Global analyses of sea surface temperature, sea ice, and night marine air temperature since the late nineteenth century. *Journal of Geophysical Research: Atmospheres*, *108*(D14). doi:

10.1029/2002JD002670

Ruprich-Robert, Y., Msadek, R., Castruccio, F., Yeager, S., Delworth, T., & Danabasoglu, G. (2016). Assessing the climate impacts of the observed Atlantic Multidecadal Variability using the GFDL CM2.1 and NCAR CESM1 global coupled models. *Journal of Climate*, *30*(8), 2785–2810. doi: 10.1175/JCLI-D-16-0127.1

Santer, B. D., Wigley, T. M. L., Boyle, J. S., Gaffen, D. J., Hnilo, J. J., Nychka, D., ... Taylor, K. E. (2000). Statistical significance of trends and trend differences in layer-average atmospheric temperature time series. *Journal of Geophysical Research: Atmospheres*, *105*(D6), 7337–7356. doi: 10.1029/1999JD901105

Schneider, D. P., & Deser, C. (2018). Tropically driven and externally forced patterns of Antarctic sea ice change: reconciling observed and modeled trends. *Climate Dynamics*, *50*(11-12), 4599–4618. doi: 10.1007/s00382-017-3893-5

Seethala, C., Norris, J. R., & Myers, T. A. (2015). How has subtropical stratocumulus and associated meteorology changed since the 1980s? *Journal of Climate*, *28*(21), 8396–8410. doi: 10.1175/JCLI-D-15-0120.1

Smith, T. M., Reynolds, R. W., Peterson, T. C., & Lawrimore, J. (2008). Improvements to NOAA's historical merged land-ocean surface temperature analysis (1880–2006). *Journal of Climate*, *21*(10), 2283–2296. doi: 10.1175/2007JCLI2100.1

Sun, T., & Okumura, Y. M. (2019). Role of stochastic atmospheric forcing from the South and North Pacific in tropical Pacific decadal variability. *Journal of Climate*, *32*(13), 4013–4038. doi: 10.1175/JCLI-D-18-0536.1

Taylor, K. E., Stouffer, R. J., & Meehl, G. A. (2011). An overview of CMIP5 and the experiment design. *Bulletin of the American Meteorological Society*, *93*(4), 485–498. doi: 10.1175/BAMS-D-11-00094.1

Tung, K.-K., & Chen, X. (2018). Understanding the recent global surface warming slowdown: a review. *Climate*, *6*(4), 82. doi: 10.3390/cli6040082

Vimont, D. J., Wallace, J. M., & Battisti, D. S. (2003). The Seasonal Footprinting Mechanism in the Pacific: Implications for ENSO. *Journal of Climate*, *16*(16), 2668–2675. doi: 10.1175/1520-0442(2003)016⟨2668:TSFMIT⟩2.0.CO;2

Wang, C., Zhang, L., Lee, S.-K., Wu, L., & Mechoso, C. R. (2014). A global perspective on CMIP5 climate model biases. *Nature Climate Change*, *4*(3), 201–

205. doi: 10.1038/nclimate2118

Wang, K., Deser, C., Sun, L., & Tomas, R. A. (2018). Fast response of the tropics to an abrupt loss of Arctic sea ice via ocean dynamics. *Geophysical Research Letters*, *45*(9), 4264–4272. doi: 10.1029/2018GL077325

Xie, S.-P., Deser, C., Vecchi, G. A., Ma, J., Teng, H., & Wittenberg, A. T. (2010). Global warming pattern formation: sea surface temperature and rainfall. *Journal of Climate*, *23*(4), 966–986. doi: 10.1175/2009JCLI3329.1

Yeager, S. G., Danabasoglu, G., Rosenbloom, N. A., Strand, W., Bates, S. C., Meehl, G. A., … Lovenduski, N. S. (2018). Predicting near-term changes in the Earth system: A large ensemble of initialized decadal prediction simulations using the Community Earth System Model. *Bulletin of the American Meteorological Society*, *99*(9), 1867–1886. doi: 10.1175/BAMS-D-17-0098.1

Zhang, H., Clement, A., & Di Nezio, P. (2014). The South Pacific Meridional Mode: a mechanism for ENSO-like variability. *Journal of Climate*, *27*(2), 769–783. doi: 10.1175/JCLI-D-13-00082.1

Zhang, L., Delworth, T. L., Cooke, W., & Yang, X. (2019). Natural variability of Southern Ocean convection as a driver of observed climate trends. *Nature Climate Change*, *9*(1), 59–65. doi: 10.1038/s41558-018-0350-3

Zhang, L., Delworth, T. L., & Zeng, F. (2017). The impact of multidecadal Atlantic meridional overturning circulation variations on the Southern Ocean. *Climate Dynamics*, *48*(5-6), 2065–2085. doi: 10.1007/s00382-016-3190-8

Figure 1.

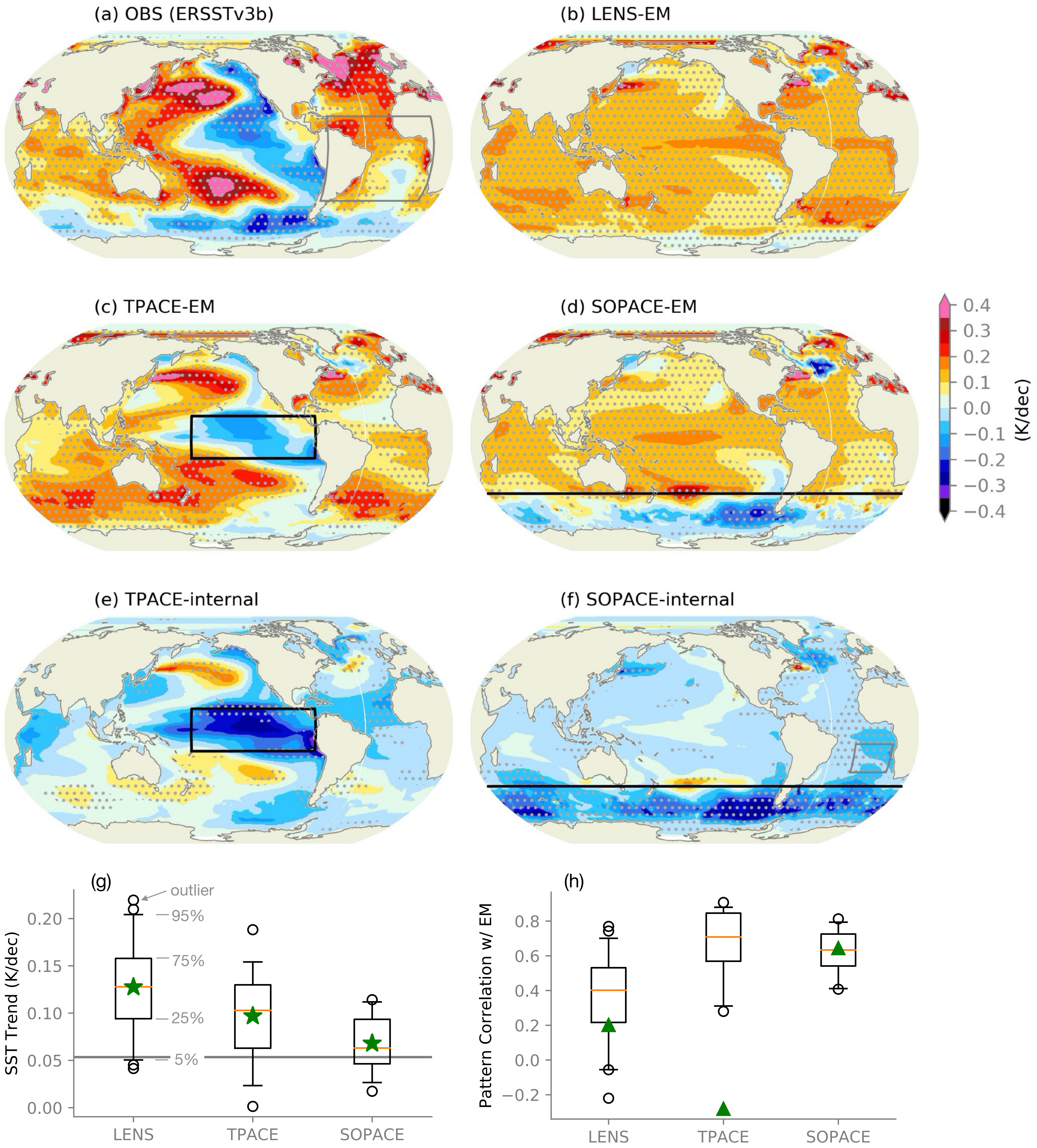

(a) OBS (ERSSTv3b)
(b) LENS-EM
(c) TPACE-EM
(d) SOPACE-EM
(e) TPACE-internal
(f) SOPACE-internal
0.4
0.3
0.2
0.1
0.0
−0.1
−0.2
−0.3
−0.4
(K/dec)
(g)
outlier
95%
75%
25%
5%
SST Trend (K/dec)
0.20
0.15
0.10
0.05
0.00
LENS
TPACE
SOPACE
(h)
Pattern Correlation w/ EM
0.8
0.6
0.4
0.2
0.0
−0.2
LENS
TPACE
SOPACE

Figure 2.

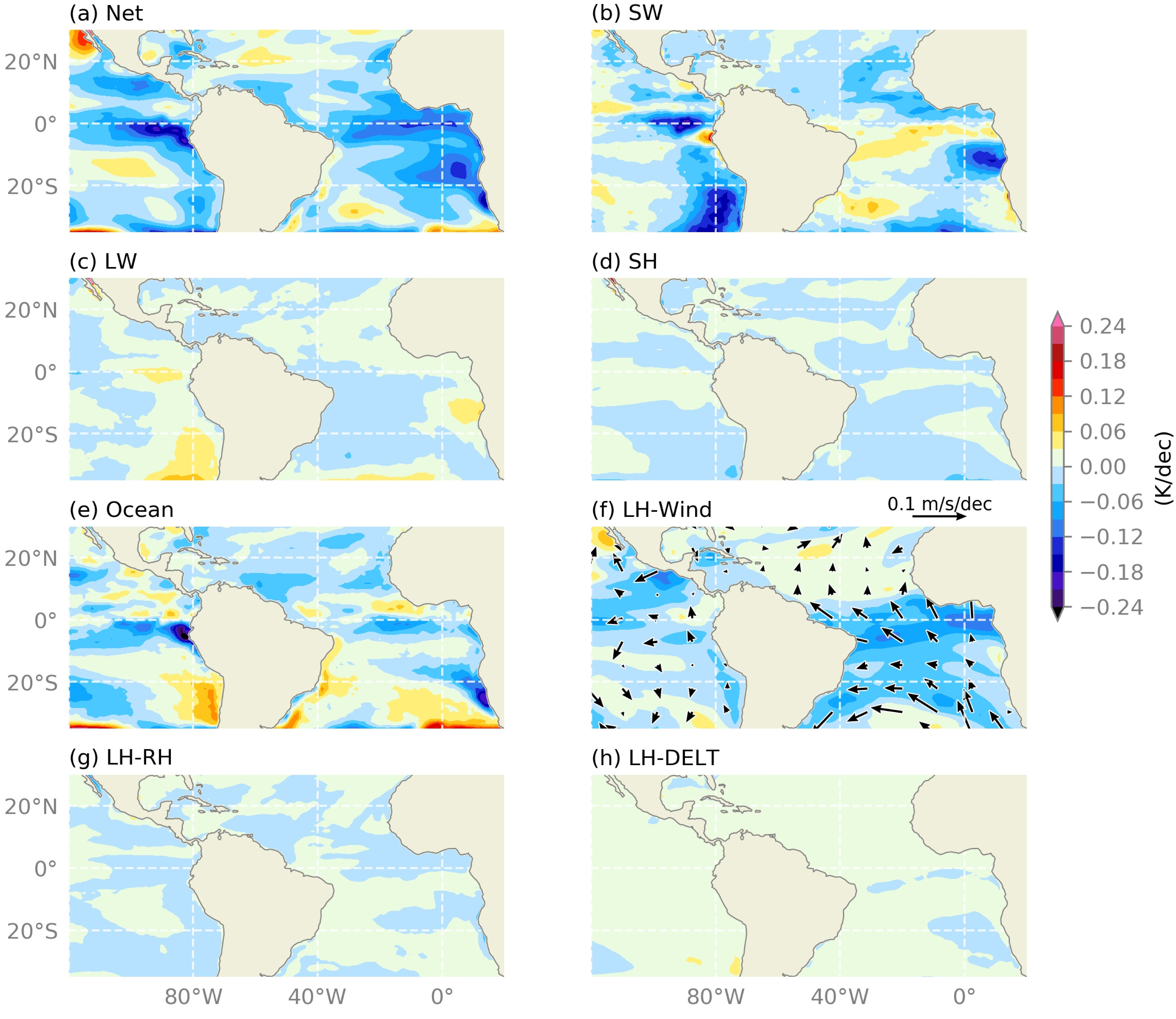
(a) Net
(b) SW
(c) LW
(d) SH
(e) Ocean
(f) LH-Wind
0.1 m/s/dec
(g) LH-RH
(h) LH-DELT
20°N
0°
20°S
80°W
40°W
0°
0.24
0.18
0.12
0.06
0.00
−0.06
−0.12
−0.18
−0.24
(K/dec)

Figure 3.

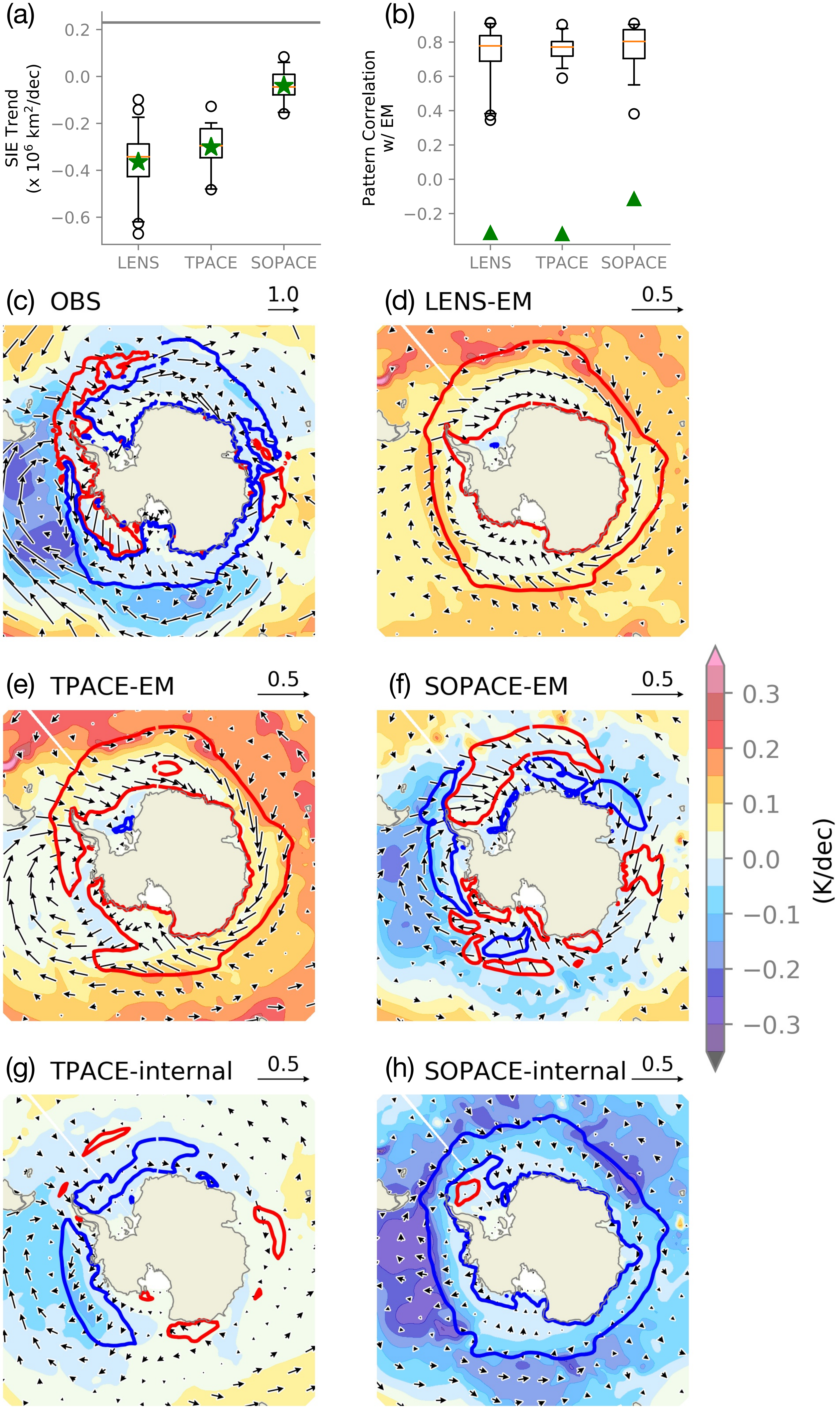
(a)
SIE Trend
(x 10^6 km^2/dec)
0.2
0.0
−0.2
−0.4
−0.6
LENS
TPACE
SOPACE
(b)
Pattern Correlation
w/ EM
0.8
0.6
0.4
0.2
0.0
−0.2
LENS
TPACE
SOPACE
(c) OBS
1.0
(d) LENS-EM
0.5
(e) TPACE-EM
0.5
(f) SOPACE-EM
0.5
(g) TPACE-internal
0.5
(h) SOPACE-internal
0.5
0.3
0.2
0.1
0.0
−0.1
−0.2
−0.3
(K/dec)

Geophysical Research Letters

Supporting Information for

Is there a tropical response to recent observed Southern Ocean cooling?

Xiyue Zhang[1], Clara Deser[1], and Lantao Sun[2]

[1]National Center for Atmospheric Research, Boulder, Colorado, USA
[2]Colorado State University, Fort Collins, Colorado, USA

Contents of this file

Text S1
Figures S1 to S6

Introduction

This supporting information provides description of our observational data sets, analysis methods, mixed layer budget equations and figures that are complementary to the main article.

Text S1.

Observational Data Sets

We use a suite of data sets to capture the observed trends during 1979-2013. SSTs are taken from the NOAA ERSSTv3b data set with 2° global resolution (Smith et al., 2008), for compatibility with those used in TPACE and SOPACE. We also show the SO SST anomaly timeseries from ERSSTv5 data set for comparison (Huang et al., 2017). The two data sets don't show significant differences in their SO SST trends (Figure S1). Surface wind data are taken from ERA-5 Reanalysis at 0.25° global resolution (Hersbach et al., 2019). Sea ice concentration data are from the passive-microwave-derived NASA Goddard Bootstrap version 2 dataset on a 25 km x 25 km grid (Peng et al., 2013).

Analysis Methods

We calculate monthly anomalies of all fields by subtracting the climatological monthly means of the 1981-2010 base period. Linear least-square regression is used to compute monthly trends during 1979-2013. We use stippling to indicate regions of statistical significance at 95% confidence level, based on a two-sided *t*-test method adjusted for autocorrelation (Santer et al., 2000; Schneider & Deser, 2018).

Ocean Mixed Layer Budget Equations

We focus on the ensemble-mean ocean mixed layer budget in SOPACE-internal, in order to isolate the forced response to the internal component of observed SO SST trends. The surface mixed-layer budget equation is:

$$\rho c_p H \frac{\partial T_s}{\partial t} = F_{\mathrm{SW}} + F_{\mathrm{LW}} + SH + LH + O. \quad \text{(S1)}$$

We can take the linear trend of Equation S1, the left-hand side which represents the trend of heat storage is negligible (Cook et al. 2018, also see Figure S3b), we will have

$$0 = F^t{}_{\mathrm{SW}} + F^t{}_{\mathrm{LW}} + SH^t + LH^t + O^t, \quad \text{(S2)}$$

where the superscript *t* denotes *linear trends* during 1979-2013.

Figure S3 shows all terms in Equation S3. The sensible heat flux trend is the smallest term. The rest of the terms can be considered forcing on SST trend $T^t{}_{\mathrm{s}}$ due to clouds ($F^t{}_{\mathrm{SW}}$), ocean dynamics (O^t), and atmospheric temperature and humidity (F^t_{LW}). The latent heat flux term directly depends on T_{s} via saturation vapor pressure:

$$LH = -L_{\mathrm{v}} c_{\mathrm{E}} \rho_{\mathrm{a}} W [q_s(T_{\mathbf{s}}) - q_{\mathrm{a}}]. \quad \text{(S3)}$$

And q_{a} is the specific humidity of air above the sea surface, thus can be written as

$$q_{\mathrm{a}} = RH_0 q_s(T_{\mathrm{s}} + \Delta T), \quad \text{(S4)}$$

where RH_0 is the relative humidity at the sea surface, and $\Delta T = T_{\mathrm{a}} - T_{\mathrm{s}}$ is the temperature gradient near the sea surface. Using the Clausius-Clapeyron equation, Equation S4 can be written as

$$q_{\mathrm{a}} = RH_0 q_{\mathrm{s}}(T_{\mathrm{s}}) e^{\alpha \Delta T}, \quad \text{(S5)}$$

Where $\alpha = \frac{L_{\mathrm{v}}}{R_{\mathrm{v}} T^2} \approx 0.06\ \mathrm{K}^{-1}$. We can plug Equation S5 into S3 and get

$$LH = -L_{\mathrm{v}} c_{\mathrm{E}} \rho_{\mathrm{a}} W (1 - RH_0 e^{\alpha \Delta T}) q_s(T_{\mathbf{s}})$$

Following Hwang et al. (2017) and Jia & Wu (2013), the linear trend of latent heat flux can therefore be linearized as

$$LH^t = \frac{\partial LH}{\partial T_s} T_s^t + \frac{\partial LH}{\partial W} W^t + \frac{\partial LH}{\partial RH_0} RH_0^t + \frac{\partial LH}{\partial \Delta T} \Delta T^t \tag{S6}$$

On the right-hand side (RHS), the last three terms can also be considered as forcing from the atmosphere due to changes in near-surface wind speed, near-surface relative humidity, and air-sea temperature gradient:

$$LH_{\mathrm{W}}^t = \frac{\partial LH}{\partial W} W^t = \overline{LH} \frac{W^t}{\overline{W}}, \tag{S7}$$

$$LH_{\mathrm{RH}}^t = \frac{\partial LH}{\partial RH_0} RH_0^t = -\frac{\overline{LH} RH_0^t}{e^{\alpha \overline{\Delta T}} - \overline{RH_0}}, \tag{S8}$$

$$LH_{\Delta \mathrm{T}}^t = \frac{\partial LH}{\partial \Delta T} \Delta T^t = \frac{\alpha \overline{LH}\, \overline{RH_0} \Delta T^t}{e^{\alpha \overline{\Delta T}} - \overline{RH_0}}, \tag{S9}$$

while the first term on RHS of Equation S6 becomes the SST damping term:

$$\frac{\partial LH}{\partial T_s} T_s^t = \alpha \overline{LH}\, T_s^t, \tag{S10}$$

where $\overline{LH}$ is the climatological mean latent heat flux, and it is negative when evaporation happens. This term in Equation S10 means that higher SST evaporates more to cool, therefore damps the temperature change. Equation S10 allows us to rewrite Equation S2 as a diagnostic equation of the SST trend:

$$T_s^t = -\frac{F^t{}_{\mathrm{SW}} + F^t{}_{\mathrm{LW}} + SH^t + O^t + LH_{\mathrm{W}}^t + LH_{\mathrm{RH}}^t + LH_{\Delta \mathrm{T}}^t}{\alpha \overline{LH}}. \tag{S11}$$

We can rewrite Equation S11 to show how different forcing terms contribute to the SST trends:

$$T_s^t = T_{\mathrm{SW}}^t + T_{\mathrm{LW}}^t + T_{\mathrm{SH}}^t + T_{\mathrm{O}}^t + T_{\mathrm{LH,w}}^t + T_{\mathrm{LH,RH}}^t + T_{\mathrm{LH,\Delta T}}^t, \tag{S12}$$

where the RHS terms can be defined using Equation S7–S9.

$$T_{\mathrm{SW}}^t = -\frac{F^t{}_{\mathrm{SW}}}{\alpha \overline{LH}}, \tag{S13}$$

$$T_{\mathrm{LW}}^t = -\frac{F^t{}_{\mathrm{LW}}}{\alpha \overline{LH}}, \tag{S14}$$

$$T_{\mathrm{SH}}^t = -\frac{F^t{}_{\mathrm{SH}}}{\alpha \overline{LH}}, \tag{S15}$$

$$T_{\mathrm{O}}^t = -\frac{F^t{}_{\mathrm{O}}}{\alpha \overline{LH}}, \tag{S16}$$

$$T^t_{\mathrm{LH,w}} = -\frac{LH^t_{\mathrm{w}}}{\alpha\overline{LH}} = -\frac{W^t}{\alpha\overline{W}}, \tag{S17}$$

$$T^t_{\mathrm{LH,RH}} = -\frac{LH^t_{\mathrm{RH}}}{\alpha\overline{LH}} = \frac{RH^t_0}{\alpha(e^{\alpha\overline{\Delta T}} - \overline{RH_0})}, \tag{S18}$$

$$T^t_{\mathrm{LH,\Delta T}} = -\frac{LH^t_{\Delta\mathrm{T}}}{\alpha\overline{LH}} = -\frac{\overline{RH_0}}{e^{\alpha\overline{\Delta T}} - \overline{RH_0}}\Delta T^t. \tag{S19}$$

Equation S12–S19 are shown in Figure 2, while the heat flux trend terms used to calculate Equation S12–S19 are shown in Figure S3.

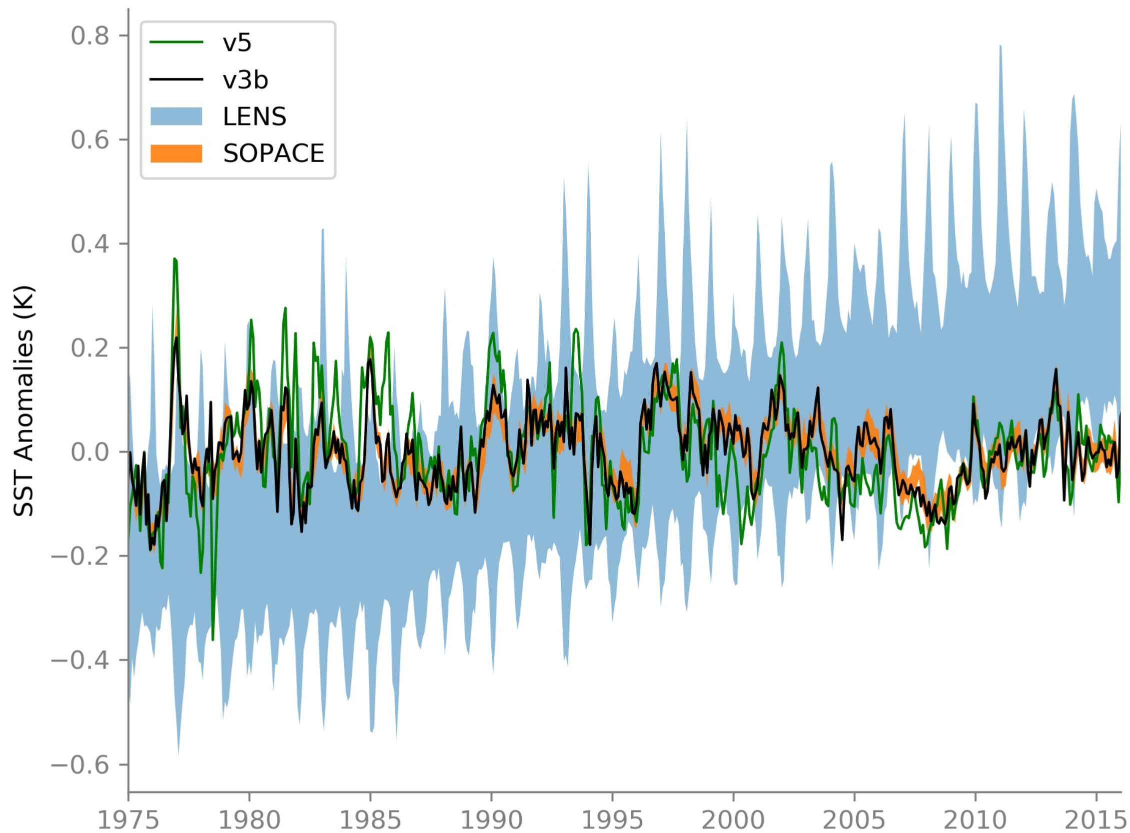

Figure S1. Southern Ocean (40-65S) averaged monthly SST anomaly from SOPACE (orange shading), LENS (blue shading), ERSSTv3b dataset (black), and ERSSTv5 (green). The 1975-2016 climatology is used to calculate the monthly anomaly.

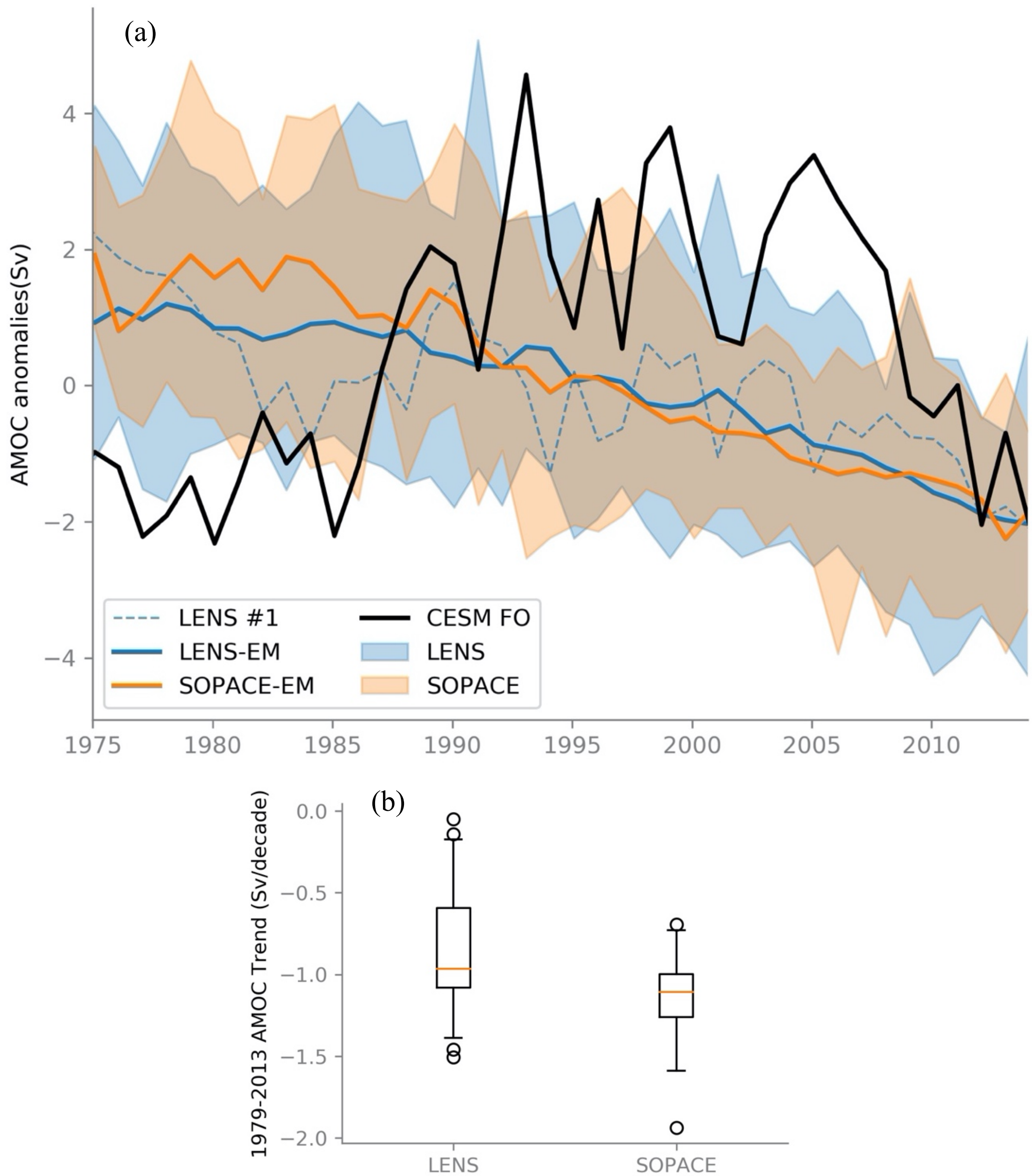

Figure S2. (a) Annual mean AMOC anomaly timeseries (defined as the maximum streamfunction value in the latitude band 20–60N and below 500 m in the Atlantic Ocean following Zhang et al. 2017). The black line shows the CESM forced ocean (FO) simulation (Yeager et al. 2018), approximating the observed AMOC timeseries. Blue solid curve shows the ensemble mean of LENS, with blue shading showing the range of the ensemble spread. Orange solid curve shows the ensemble mean of SOPACE, with orange shading showing the range of the ensemble spread. The dashed blue curve shows the first ensemble member of LENS, which was used to initialize all 20 members of SOPACE. The 1975-2016 climatology is used to calculate the monthly anomaly. (b)

Box and whisker plot of AMOC trend (1979-2013) from LENS and SOPACE ensemble members. Orange lines show the median values, boxes show the middle 50% members, whiskers show the 5 to 95% members, and circles show the outliers.

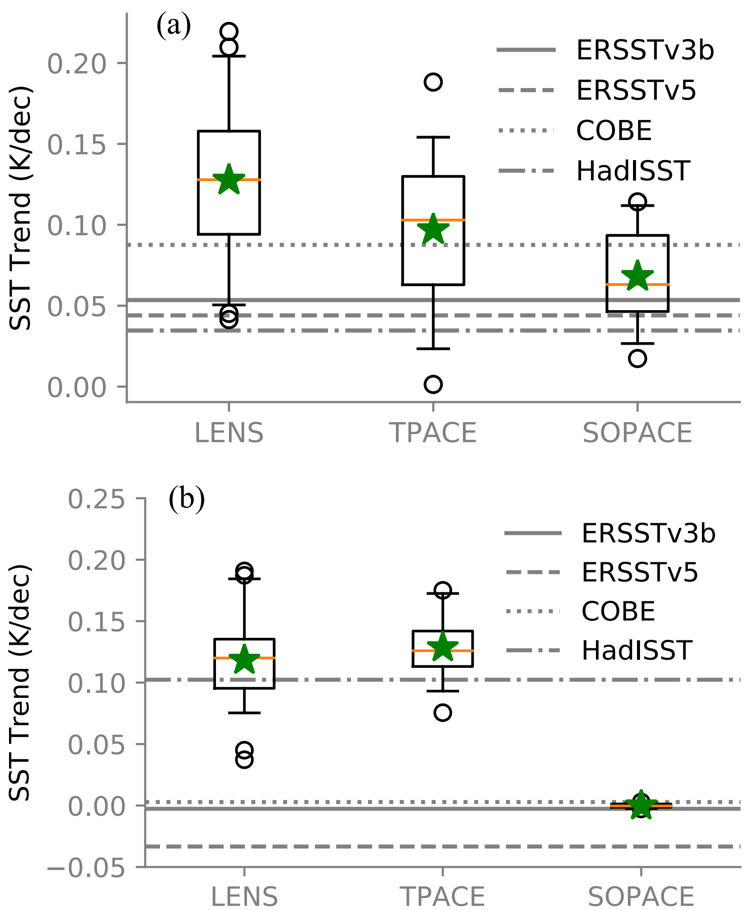

Figure S3. Box-and-whisker plot of SST trends averaged over (a) tropical South Atlantic (gray box in Figure 1f) and (b) the Southern Ocean (40S-65S) for each model ensemble. Green stars show the EM values. Orange lines show the median values. Gray horizontal lines show the observed values from various data sets: NOAA Extended Reconstruction SSTs version 3b and 5 (ERSSTv3b & ERSSTv5, Huang et al. 2017), Centennial in situ Observation-Based Estimates (COBE, Ishii et al. 2005), and the Hadley Centre Global Sea Ice and Sea Surface Temperature (HadISST, Rayner et al. 2003).

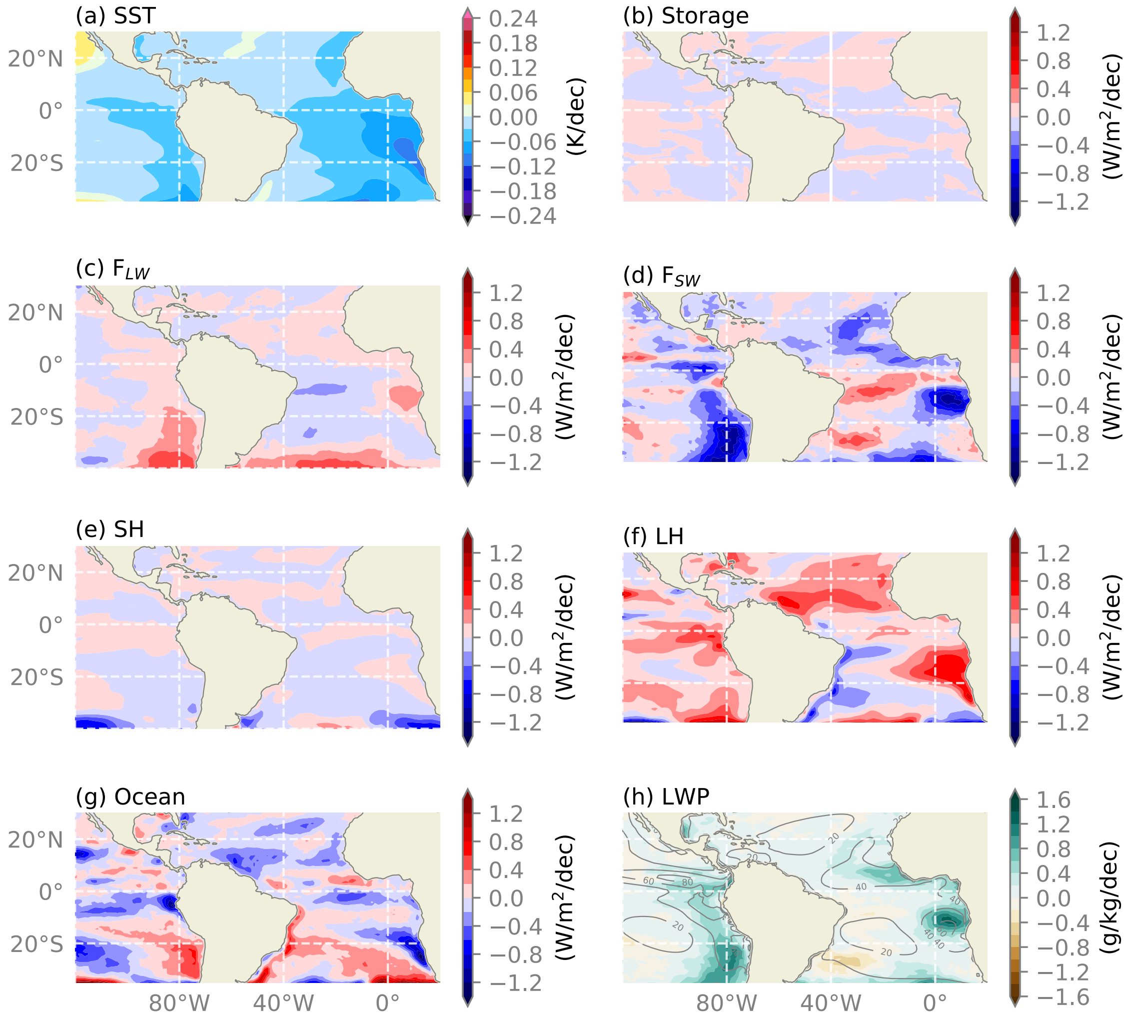

Figure S4. Terms in the ocean mixed layer heat budget based on monthly trends during 1979–2013 from SOPACE-internal over the tropical eastern Pacific and Atlantic. (a) SST trend, (b) trend in mixed layer heat storage (left hand side of equation (1)), (c) net longwave flux trend, (d) net shortwave flux trend, (e) sensible heat flux trend, (f) latent heat flux trend, (g) trend due to ocean dynamics, and (h) trend in liquid water path (contours show the climatological LWP). Positive flux is downward and warms the SST.

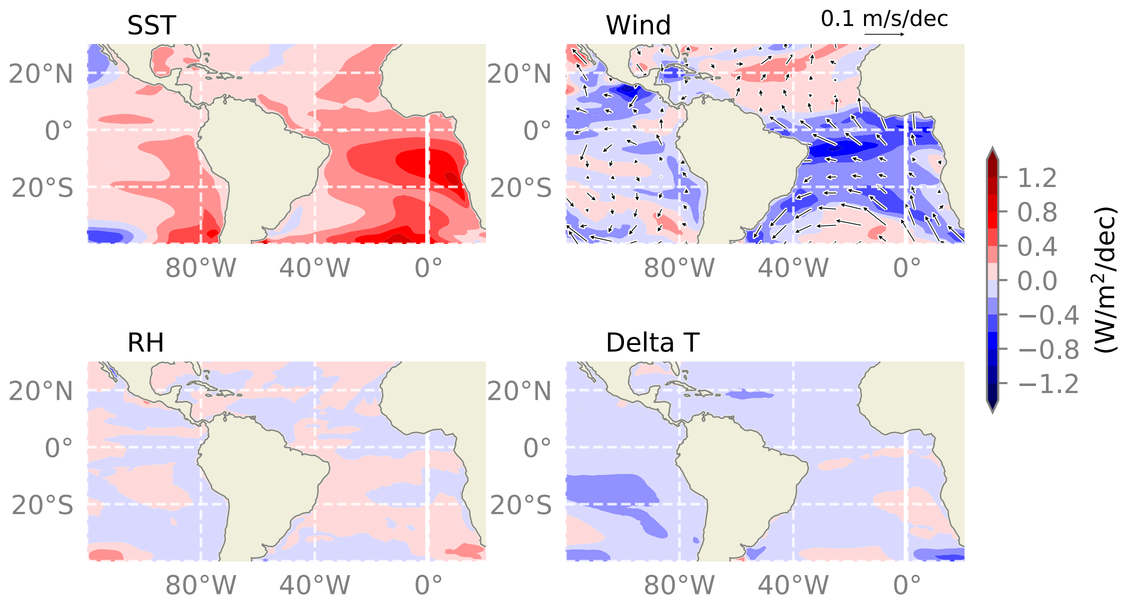

Figure S5. Latent heat budget based on monthly trends during 1979—2013 from SOPACE-internal over the tropical eastern Pacific and Atlantic due to (a) SST damping, (b) near-surface wind speed changes, (c) near-surface relative humidity changes, and (d) air-sea temperature difference changes. See Equation S6 for details.

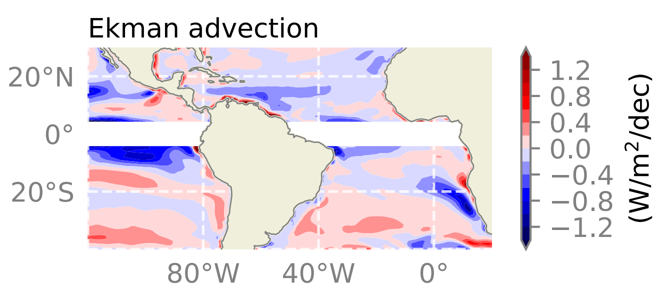

Figure S6. Ekman advection based on monthly trends during 1979—2013 from SOPACE-internal over the tropical eastern Pacific and Atlantic, expressed as an equivalent surface heat flux trend. Area near the equator (5°S–5°N) is masked out.